Tectonics

RESEARCH ARTICLE
10.1029/2017TC004917

Key Points:
- High-resolution slip histories for blind thrust faults in the Northern Apennines are reconstructed using growth strata
- Each of the investigated faults exhibits variable slip behavior over a range of time scales
- Fault slip rate variability on disconnected thrusts is asynchronous and independent of external boundary conditions at intermediate time scales

Supporting Information:
- Table S1
- Table S2

Correspondence to:
K. L. Gunderson,
kgunderson@chevron.com

Citation:
Gunderson, K. L., Anastasio, D. J., Pazzaglia, F. J., & Kodama, K. P. (2018). Intrinsically variable blind thrust faulting. *Tectonics*, *37*, 1454–1471. https://doi.org/10.1029/2017TC004917

Received 2 DEC 2017
Accepted 18 APR 2018
Accepted article online 30 APR 2018
Published online 19 MAY 2018

Intrinsically Variable Blind Thrust Faulting

Kellen L. Gunderson[1,2], David J. Anastasio[1], Frank J. Pazzaglia[1], and Kenneth P. Kodama[1]

[1]Department of Earth and Environmental Sciences, Lehigh University, Bethlehem, PA, USA, [2]Chevron Energy Technology Company, Houston, TX, USA

Abstract We propose that most fault slip rate variability across a range of time and spatial scales is due to intrinsic faulting processes, rather than extrinsic changes in surface loads or stress boundary conditions. This hypothesis is tested by comparing very high geologic resolution slip histories of blind thrust faults from three transects in the Northern Apennines, Italy. We investigated whether these slip histories document synchronous, or independent, behavior of the disconnected, blind thrust faults that core mountain front anticlines bordering the Po foreland. The slip history for these thrusts is reconstructed by applying forward structural modeling to deformed growth strata and fluvial terraces preserved on the limbs of the growing anticlines. We present a new age model using magnetostratigraphy and cyclostratigraphy for a section of growth strata exposed in the Panaro River and supplement this with age models for two other published transects. The blind thrust fault at each transect exhibits variable slip behavior over the past 3 Myr, but for most of that time the variability was both asynchronous and independent of boundary condition changes, such as Plio-Pleistocene sediment accumulation variability. However, a major deceleration in slip rates at all three locations is temporally coincident with the overfilling of the Po foreland beginning in the early Pleistocene. We attribute the deceleration to a switch from shortening on shallowly detached thrusts to shortening on a crustal-scale basement-involved fault. This switch has implications for the time and spatial scales at which extrinsic boundary conditions may contribute to deformation variability.

1. Introduction

It is now recognized that faults commonly exhibit both unsteady and nonuniform slip behavior across a range of space and time scales (collectively referred to as variable slip behavior; Dolan et al., 2016; Dolan & Meade, 2017; Gold & Cowgill, 2011; Gold et al., 2017). This variability has been observed in all tectonic settings in both field and model studies (Cowie et al., 1993, 2012; Friedrich et al., 2003; Rogers & Dragert, 2003; Mouslopoulou et al., 2009; Naylor & Sinclair, 2007; Saint-Charlier et al., 2016). Compilations of long-term, high-resolution deformation records reveal the characteristic time scales of fault slip rate variability, but there is still no clear theoretical framework that explains the controlling mechanisms or apportions the relative influence of intrinsic processes, such as fault mechanical behavior, versus extrinsic forcing, such as tectonic or climatic surface loads changing the stress boundary conditions (Dolan et al., 2016). Understanding the underlying processes of fault slip rate variability is important because, among other reasons, earthquake hazard assessments that rely on the slip predictable or time predictable models of fault behavior assume that fault slip rates should be constant (steady and uniform) when averaged over multiple seismic cycles (Wallace, 1987).

The observed slip rate variability over intermediate (10^4–10^6 years) time scales that span multiple seismic cycles and link instrumental to geologic observations leads to interesting questions regarding intrinsic process versus extrinsic forcing as modulators for the observed fault slip rate variability. For instance, if slip rates are variable over 10^4–10^6 year time scales does this signify similar extrinsic temporal changes in the fault's boundary conditions responding to far-field tectonic forcing or climate-driven changes in erosion and deposition of an orogenic wedge? Alternatively, if it is assumed that boundary conditions remain constant over these time spans, does the presence of slip rate variability imply that these variations are driven by processes intrinsic to the fault network, such as strain hardening as a fault elongates, the evolutionary focusing of displacement on the structurally mature fault plane (Dolan & Haravitch, 2014), or that slip is partitioned on connected structures? Several hypotheses have emerged to explain these possible behaviors. One is that a tectonic megaoscillator (Davis et al., 2006) modulates crustal-scale energy transfer through the interaction of stresses induced by surface waves and magma or groundwater in the crust (Brodsky et al., 2003) or from large-scale stress diffusion in the mantle following clusters of great earthquakes (Pollitz et al., 1998). A logical and intriguing extension of the megaoscillator idea is that surface processes, such as climate change, can also drive variations in groundwater flow or the distribution of mass at the surface and thus modulate stress changes (Chéry & Vernant, 2006; Hampel et al., 2010; Hetzel & Hampel, 2005). Similarly, at the short time scales represented by episodic slip and tremor events, a resonance response to environmentally driven stress perturbations has been invoked to explain the periodic behavior of these events at diverse locations and why slip is focused near the base of the seismogenic zone (Lowry, 2006). At longer time scales, field studies and models have demonstrated that surface processes redistribute mass at the Earth's surface, which can modify the stress state on faults and thereby influence the rates and locus of deformation in orogenic wedges (Simpson, 2006).

Here we present the results of a natural experiment that provides insight into how intrinsic fault processes and extrinsic surface loads conspire to drive variable fault slip at 10^4–10^6 year time scales, expressed as the duration, timing, and growth rate on three disconnected, strike-parallel, blind thrust cored anticlines at the northern Apennine mountain front. We determined slip rates for these faults using passive stratigraphic and geomorphic markers such as growth strata and fluvial terraces. These markers provide records of fold growth and kinematics (Gunderson et al., 2013; Wilson et al., 2009), which were inverted for slip on the underlying faults using kinematic modeling techniques. The natural experiment presented here overcomes the problems of resolution and record length that limit Global Positioning System (GPS) and paleoseismic approaches and allows us to compare the overlapping deformational records for disconnected structures that are subject to the same regional boundary conditions. Our approach allows us to test if the observed deformational variability has a periodicity in phase with known extrinsic surface load forcings, like erosion and sedimentation that respond to orbitally driven climatic changes (Hetzel & Hampel, 2005), or if it is entirely intrinsic to the fault system and simply the expected behavior of the complex arrangement of faults in an orogenic wedge (Langer et al., 1996; Stein et al., 1994). It is important to clarify that we are not appealing to a specific geodynamic process; rather, we are envisioning the broader context of well-known individual fault dynamics and fault interactions with erosion and deposition throughout an actively deforming orogen as influencing the crustal-scale stress field to drive the slip variability on individual faults.

1.1. Geologic Setting

The Northern Apennines are an accretionary fold and thrust belt resulting from the ongoing subduction of Adria (Carminati & Doglioni, 2012). Geologic data (Cavinato & De Celles, 1999), including the total length of the subducted slab (Benoit et al., 2011), suggest that the long-term rate of subduction and migration of deformation into foreland is ~10 mm/year. GPS-geodesy (Bennett et al., 2012) and seismicity (Pondrelli et al., 2006) show that the current rate of shortening across the Apennine foreland is accommodated by structures at or near the northern Apennine mountain front at ~3 mm/year, consistent with the long-term rate of shortening in the context of the structural front migration rate (Basili & Barba, 2007), and indicates that the large-scale tectonic boundary conditions on this orogen have been steady for the past ~20 Ma. The Northern Apennines (Figure 1) consist of a series of thrust sheets, partially capped by the Liguran structural lid, that have propagated into and imbricated the southern half of the Po foreland basin (Ricci Lucchi, 1986). The Plio-Pleistocene Po Basin stratigraphy represents the most recent of several foreland basin stratigraphic successions that stretch back to the late Eocene (Figure 1). The Po foreland records a transition from marine to terrestrial environments in the Pleistocene where the rate of sediment accumulation and flux is shown to vary with Alpine glaciations (Ghielmi et al., 2010). Both terrestrial and marine Po foreland strata display growth geometries that record the progressive deformation of Apennine structures (Argnani et al., 2003; Artoni et al., 2004).

The relief of the modern-day topographic northern Apennine mountain front results from active deformation on blind thrust anticlines that also expose proximal Plio-Pleistocene foreland dipping growth strata on the anticlinal forelimbs. We use exposures of syngrowth deposits in the Salsomaggiore, Enza, and Panaro River valleys (S, E, and P in Figure 1) associated with three different leading-edge anticlines to reconstruct fault slip along different segments of the northern Apennine mountain front (Figure 2). The mountain front at the Stirone (western) transect is underlain by the Salsomaggiore anticline (Figure 2a), a doubly plunging fault propagation fold that is cored by Miocene sandstone (Artoni et al., 2004). The progressive deformation of the mountain front here is recorded by Plio-Pleistocene growth strata (Gunderson et al., 2012) and uplifted fluvial terraces (Wilson et al., 2009) exposed in the Stirone River valley. The mountain front at the Enza (central) transect coincides with the Quattro Castella anticline (Figure 2b; Argnani et al., 2003), and deformation of the mountain front here is recorded by growth strata in the Enza River (Gunderson et al., 2014) and fluvial

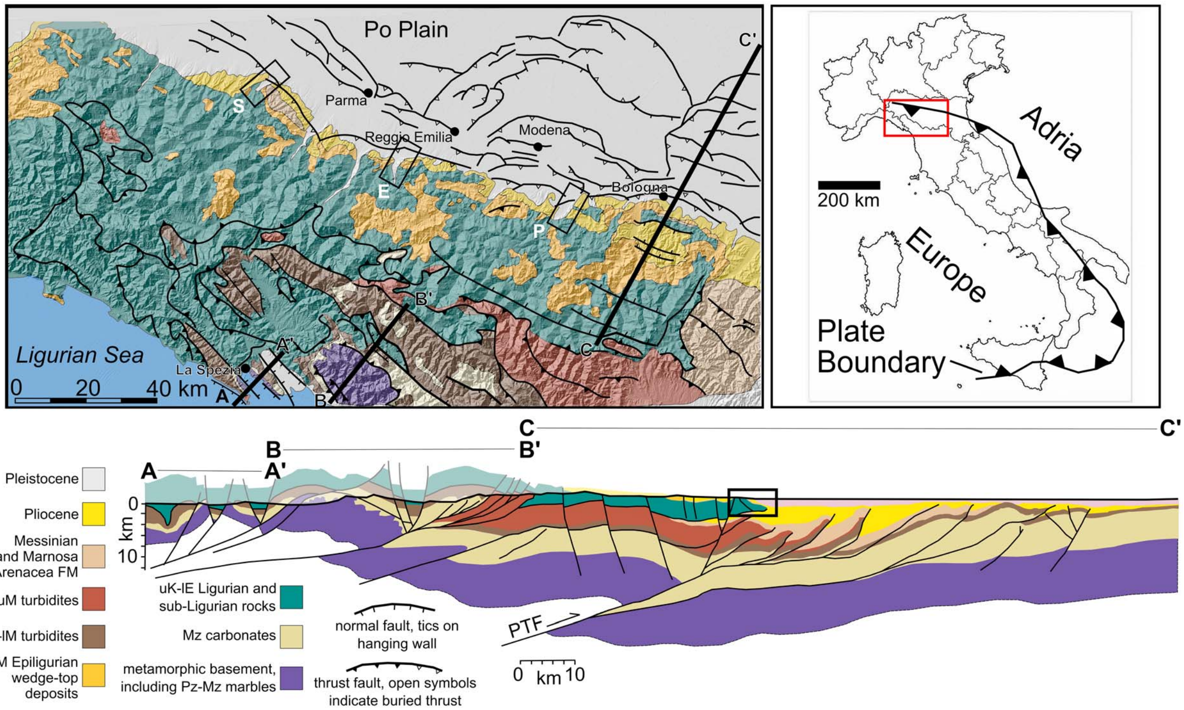

Figure 1. (top) Geologic map of the study area in the Northern Apennines (compiled from Picotti & Pazzaglia, 2008; Vannucchi et al., 2008). Location of this map is shown in the red box on the regional map to the right. The locations of the three transects from this study are outlined by the black boxes on the geologic map: S—Stirone, E—Enza, P—Panaro. (bottom) Composite cross section across the Northern Apennines and Po Plain. The transects from this study are located at the modern topographic mountain front at the margin of the Po Plain, as outlined by the black box in the cross section. PTF = Pedeapenninic Thrust Fault. The cross section is a composite projection of the three lines and therefore does not correspond precisely to the map, particularly where the lines terminate.

terraces exposed on the anticlinal forelimb (Ponza et al., 2010). Mountain front relief at the Panaro (eastern) transect is due to deformation of the Castelvetro anticline. Growth strata exposed in the Panaro River (this study) and fluvial terraces above the Castelvetro anticline (Figure 2c; Ponza et al., 2010) record the deformational history of the mountain front at this location. The geometry of all three structures are well constrained from industry seismic data and wells (Oppo et al., 2013, 2015). A recent uplift of the entire orogenic wedge, including the fault-related folds described above, is proposed to have resulted from post-Pliocene slip on the Pedeapenninic thrust fault (PTF), which is a crustal-scale, thick-skinned fault (Boccaletti et al., 1985; Picotti & Pazzaglia, 2008).

In summary, apart from the long, continuous exposures of foreland-dipping growth strata and fluvial terraces in the river valleys, there is nothing special or different about the tectonic development of the Apennine fold and thrust belt that biases its constitutive structures toward deformational variability. Because of the proximity of the Po foreland to the Alps and its history of climate-related surface processes variability, the Apennine orogenic wedge provides a mountain belt where the influence of surface processes as an extrinsic driver of slip rate variability can be tested for both thin-skinned and thick-skinned structures in a tectonically active region.

2. Methods

2.1. Magnetostratigraphy and Cyclostratigraphy

We used progressively folded growth strata and fluvial terraces to measure the deformational history of the three blind thrust faults in this study. Robust, high-resolution age models for the Stirone section, the Enza section, and the fluvial terraces were developed in previous studies (Gunderson et al., 2012, 2014). We supplement those studies with a new age model for the Plio-Pleistocene Panaro River stratigraphic section using magnetostratigraphy and cyclostratigraphy, following the same methodology that was applied to the Stirone and Enza studies (Gunderson et al., 2012, 2014).

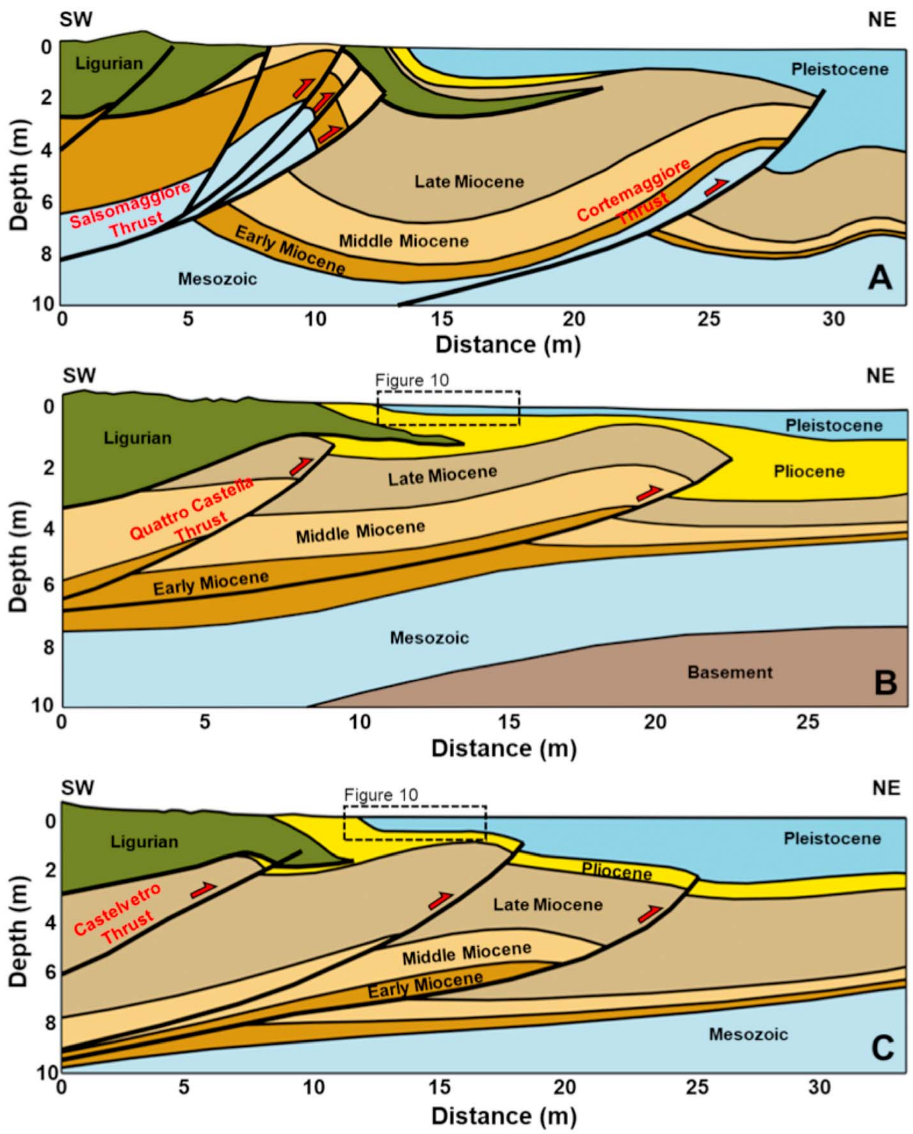

Figure 2. Structural cross sections for the Stirone (a), Enza (b), and Panaro (c) transects modified from Oppo et al. (2013). Cross sections are constrained by publicly available seismic and well data. The dashed black boxes in Figures 2b and 2c show the extent of dated growth strata that were correlated into the subsurface.

We collected stratigraphic, structural, rock-magnetic, and paleomagnetic data for a 538-m thick stratigraphic section deposited on the forelimb of the Castelvetro fault-related fold along the Panaro River corridor near the town of Vignola (Figure 3). The lithology was described at 1-m spacing, and bedding orientations were recorded at every paleomagnetic sample location and at any point where there was an obvious change in bedding orientation. Oriented samples were collected for paleomagnetic analysis at 52 horizons with an average stratigraphic spacing between sites of ~10 m. At least three oriented samples were collected at each horizon in plastic boxes from pedestals carved into the outcrop. We subjected 127 samples to alternating field demagnetization from 0 to 100 mT in 10-mT steps and 29 samples to thermal demagnetization from 0 to 600°C in 50°C steps. The number of samples subjected to thermal demagnetization was limited to the samples that could be removed from their plastic boxes for the progressive heating without being compromised. The characteristic remanent magnetization (ChRM) directions were determined by principal component analysis (Kirschvink, 1980). We then determined the virtual geomagnetic poles (VGPs) from the remanence directions and calculated mean horizon VGPs using Fisher statistics (Fisher, 1953). The VGPs were then used to define magnetozones of the same polarity, and each magnetozone was correlated to the geomagnetic polarity time scale of Gradstein et al. (2012). We also collected unoriented samples every 1.5 m for

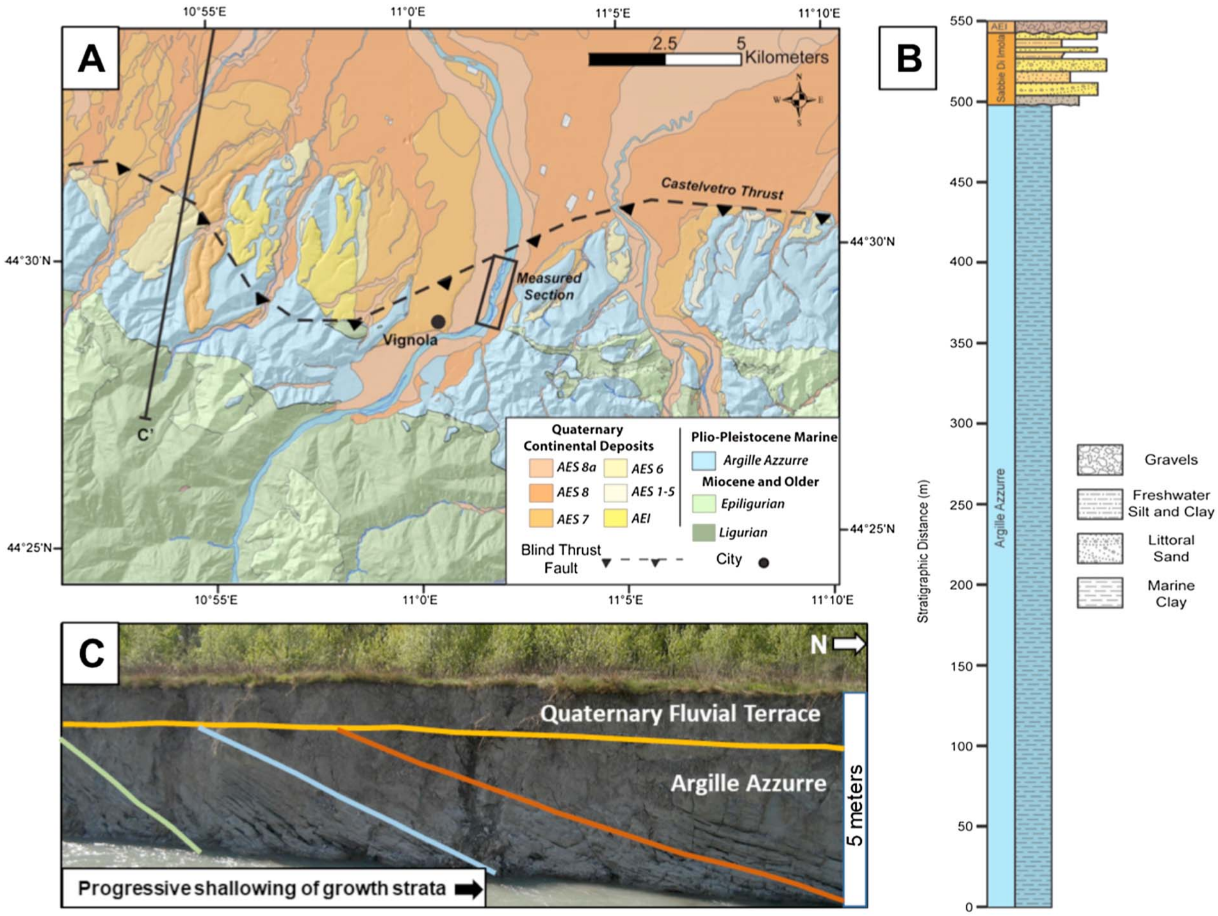

Figure 3. (a) Bedrock and surficial geologic map of the area near Vignola. The location of the measured Plio-Pleistocene growth section exposed in the Panaro River is shown in the black box. In this area, the shallow thrust fault responsible for deformation of the Apennine mountain front is known as the Castelvetro thrust. West of the measured section there is a suite of uplifted and incised fluvial terraces (Associazione Emilia-Romagna Inferiore, AEI, or Superiore, AES, deposits) that record the middle to late Pleistocene deformation of the Castelvetro thrust (see main text). (b) Stratigraphy of the Plio-Pleisocene Panaro section. (c) Photography of foreland dipping growth strata exposed along the Panaro River illustrating the continuous exposure and progressive folding of the stratigraphy.

rock-magnetic cyclostratigraphy between 0 and 498 m in the Argille Azzurre Fm. and measured low-field magnetic susceptibility (χ) for each sample on a KLY-3S Kappabridge at Lehigh University. Each χ measurement was normalized by sample mass.

We used multitaper method (MTM) spectral analyses (Thompson, 1982, 1990) using the SSA-MTM software (Ghil et al., 2002) to identify significant climate-related periodicities in the absolute time-calibrated χ data series, using a steady sedimentation rate within each magnetic chron set by the reversal stratigraphy. We considered a spectral peak as significant if the power exceeded a 95% confidence interval above a robust red noise model (Mann & Lees, 1996). After identifying significant cycles at ~1/40-kyr frequency, we correlated peaks in the χ data series to the peaks in the theoretical obliquity model from Laskar et al. (2004) to refine the assigned stratigraphic ages.

2.2. Structural Modeling

We used the progressive folding of growth strata and the uplift of fluvial terraces as proxies for slip on the underlying faults at each structure. Suppe et al. (1992) demonstrated that growth strata can be used to determine fault slip in fault-related folds in many settings, and Gunderson et al. (2013) used surface measurements of growth strata from the Stirone section (Figure 2), along with geometric constraints from subsurface seismic data to model slip on the Salsomaggiore thrust fault. Gunderson et al. (2013) demonstrated that the observed surface and subsurface growth strata geometries can be reproduced by applying trishear kinematics

10.1029/2017TC004917

(Erslev, 1991) to the Salsomaggiore thrust. Additionally, the results of that study showed a strong linear relationship between the degree of limb rotation observed in the growth strata at the surface and the amount of fault slip calculated for each horizon. So even though the surface measurements of bedding dip cannot independently or uniquely resolve slip on a blind thrust, simple application of well-accepted fault-related folding kinematic models quickly reduces the degrees of freedom and allows surface measurements of growth strata to be interpreted in terms of fault slip.

We followed an approach similar to Gunderson et al. (2013) in building structural models for the Enza and Panaro sections. First, we correlated growth strata measured at the surface into the subsurface using cross sections that were constructed with publicly available seismic and well data (Figure 2; Oppo et al., 2013, 2015) to constrain the subsurface geometry and the location of the fault tips. A series of forward models were then created that modeled slip on the blind thrusts with folding occurring in the growth strata above the fault tips using trishear fault-related folding kinematics (Erslev, 1991) to replicate the interpreted surface and subsurface geometry. We systematically varied the trishear variables to find best fit values for each of the parameters, similar to the Monte Carlo approach employed by Oakley and Fisher (2015) or the grid search approach of Allmendinger (1998). Because the total amount of slip and the position of the fault tip were determined by the seismic-based cross sections, the trishear parameters were tightly constrained in this study. While we had extremely high geochronologic resolution of the growth strata afforded to us by our cyclostratigraphy, we were unable to model every single dated growth horizon because the structural resolution afforded by subsurface correlation was too coarse. Instead, we progressively modeled the deformation of major formation contacts and/or horizons dated from magnetostratigraphy and used the empirical relationship between the measured bed dip and modeled fault slip for those horizons to calculate the fault slip needed to deform horizons at higher resolution than our structural model.

Records of deformation at each of the transects for the last ~700 kyr were compiled using deformed fluvial terraces. Fluvial terraces similarly serve as passive markers of deformation and can be used to determine slip rates on blind thrust faults (e.g., Lavé & Avouac, 2001). The terraces allow us to record deformation on the same structures as the growth strata in the time since the Po Basin filled and deposition of marine growth strata ceased, albeit at a coarser resolution. In this study, we compile and compare records of river incision from terraces from studies by Wilson et al. (2009) and Ponza et al. (2010). The growth strata and the fluvial terraces records are combined to compile ~3-Myr-long records of deformation at three locations along strike (Figure 1).

3. Results

3.1. Lithostratigraphy and Magnetostratigraphy

Two major lithostratigraphic units are represented in the Panaro growth section (Figure 3). From 0 to 498 m, the section consists of homogenous, thickly bedded, blue-gray neritic clays of the Pliocene-early Pleistocene Argille Azzurre Fm. Unconformably overlying the Argille Azzurre Fm. is ~40 m of early to middle Pleistocene interbedded, cross-bedded, medium grained, littoral yellow sands and freshwater muds known of the Sabbie di Imola Fm. The Sabbie di Imola Fm. is topped by an unconformity that bounds a stratified fluvial gravel deposit that belongs to the middle to late Pleistocene Associazione Emilia-Romagna Inferiore or Superiore units (Amorosi & Pavesi, 2010). Bedding dips across the investigated interval progressively shallow, consistent with syndeformational deposition. Bedding dips are 59°NE toward the foreland at the base of the exposed section in the Argille Azzurre Fm. and progressively shallow to 21°NE toward the foreland in the Sabbie di Imola Fm. The comparative lithostratigraphy for the Stirone and Enza sections are found in Gunderson et al. (2012, 2014) respectively.

Principal component analysis successfully isolates the ChRM directions in 148 out of 156 (95%) paleomagnetic samples. Vector endpoint diagrams for representative samples are shown in Figure 4. The number of magnetic components is not consistent across all of the samples; some have a single component of magnetization, while others have multiple components (Figure 4). Thermal and AF demagnetization curves suggest the presence of both magnetite and greigite as remanence carriers, though greigite is more common. Greigite is recognized in lithologically and chronologically equivalent sections as a primary carrier of magnetic remanence (Gunderson et al., 2012; Mary et al., 1993; Sagnotti & Winkler, 1999). In many of the samples subjected to AF demagnetization, a high-coercivity overprint component of magnetization, likely also

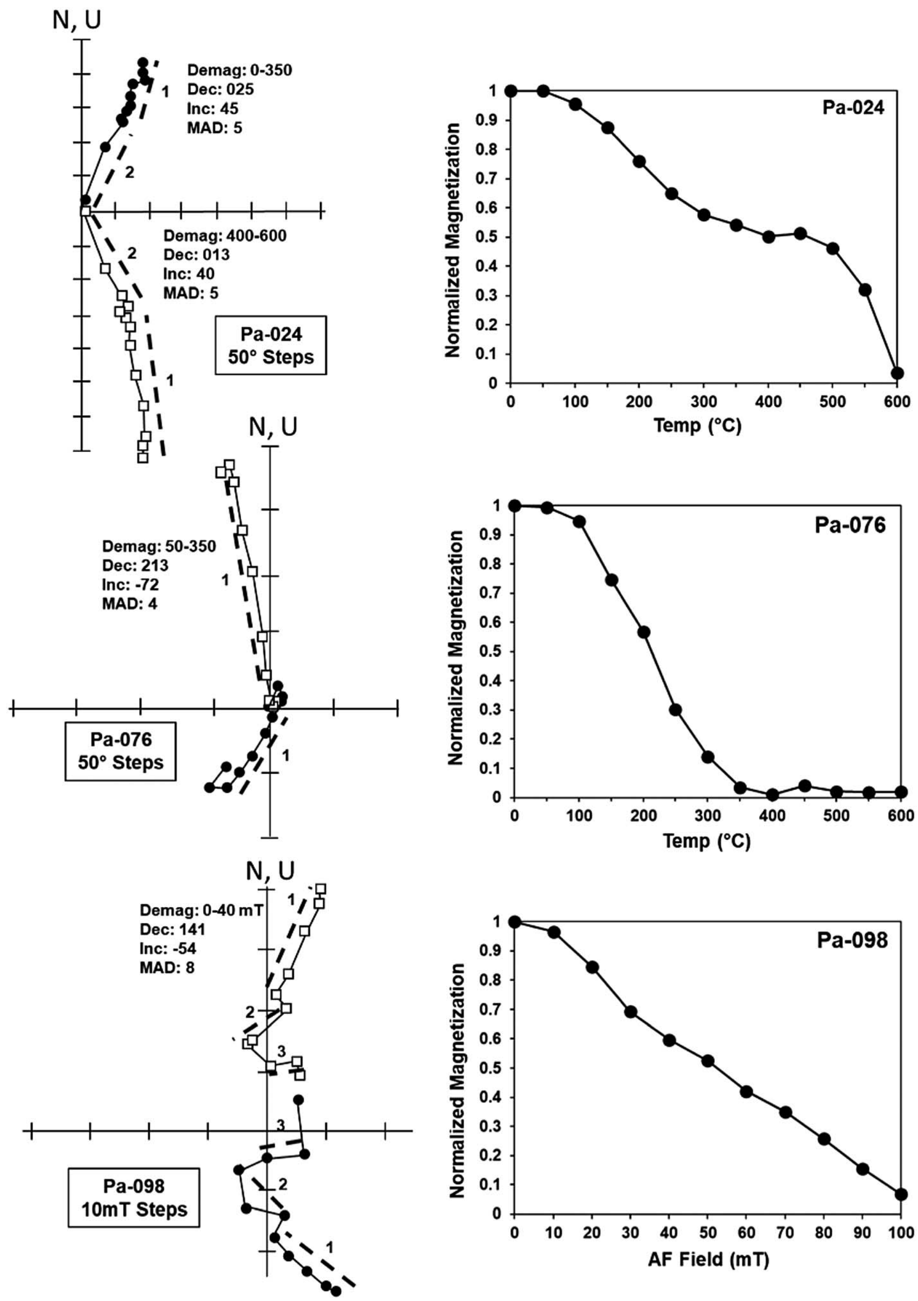

Figure 4. Vector endpoint diagrams (Zijderveld, 1967) and progressive demagnetization curves for representative samples from the Panaro section that show the range of paleomagnetic data quality and the major magnetic components. Open squares represent the vertical component of magnetization, and the filled circles represent the horizontal component in the vector endpoint diagrams. Samples Pa-024 and Pa-076 were subject to progressive thermal demagnetization , while Pa-098 was subject to alternating field (AF) demagnetization. The progressive demagnetization curves suggest the presence of both magnetite (Pa-024) and iron-sulfide (Pa-076) minerals. Pa-024 shows a ChRM that represents a normal polarity primary magnetization. Pa-076 shows a ChRM that represents a reverse polarity primary magnetization. Pa-098 shows multiple components of magnetization, a primary low coercivity (reverse polarity) component and 1–2 high-coercivity components in random orientations.

representing greigite, is present (Figure 4); this unstable overprint component is not recognized in the thermal demagnetization samples.

The remanent directions obtained from principal component analysis are shown in Figure 5 and in Table S1 in the supporting information. There are three major groups of component directions recognized: (1) a north and down orientation interpreted to represent a primary normal polarity, (2) a south and up orientation

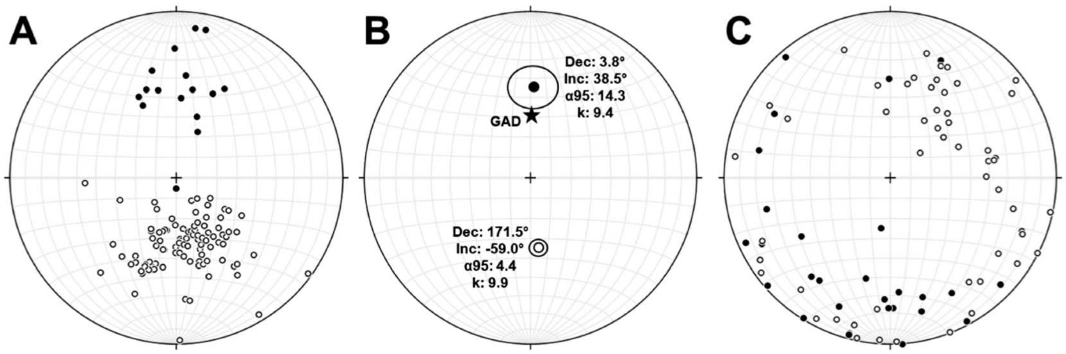

Figure 5. Equal area projections of magnetization directions. Filled circles represent a positive inclination, open circles represent a negative inclination. (a) Characteristic remanent magnetization (ChRM) directions for all samples from the Panaro section. (b) Mean remanent magnetization directions with 95% confidence ellipses. GAD- geocentric axial dipole field. (c) Randomly oriented directions obtained from the overprint components that are observed in many samples.

interpreted to represent a primary reverse polarity, and (3) a series of random oriented directions that represent a magnetization overprint. The first two directions are interpreted as the ChRM directions. The overprint component can be split into two groups; a few of the samples containing this component have a complete overprint of the primary magnetization. These samples tend to have a north and up overprint direction. But for most of the samples that have an overprint component, it is a partial overprint with random orientations that span the higher coercivity ranges (Figure 4). For the samples that are interpreted to have a primary ChRM, a reversal test shows that the north and down (first) and south and up (second) directions' 95% confidence intervals partially overlap, indicating that these directions are roughly antipodal and that they are primary remanent directions that capture reversals of the Earth's magnetic field. Additionally, while a true fold test cannot be performed because all of the magnetostratigraphy came from a single limb of the fold, the normal and reverse polarity samples show better clustering in their tilt-corrected directions than in their geographical directions, supporting the interpretation that the ChRM's used in the magnetostratigraphy represent the primary remanent directions. Samples in which the ChRM remanent direction is unknown due to overprinting (i.e., north and up directions) were not used in magnetostratigraphy.

VGP latitudes were calculated for each normal and reverse polarity sample. Based on the average VGP latitude for each sample horizon, eight magnetozones and their proposed correlation to the geomagnetic polarity time scale (Gradstein et al., 2012) are defined for the Panaro section (Figure 6). Three intervals show intermediate VGP latitudes where no polarity can be conclusively defined. The correlation is anchored by the assignment of the part of the R4 magnetozone that encompasses the Sabbie di Imola to the C1r.1r (Matuyama) subchron. Magnetostratigraphy of the Enza section (Gunderson et al., 2014) indicated that Sabbie di Imola in that section spanned both the C1r.1r and C1r.1n (Jaramillo) subchron within the Matuyama chron. In contrast, for the Panaro section we interpret that the time encompassing the Jaramillo subchron within R4 is lost in the unconformity at the base of the Sabbie di Imola. Assuming this unconformity does not consume all of the time of the R4 magnetozone, and the section below the unconformity, which is all Argille Azzurre Fm, corresponds to C1r.2r subchron. This interpretation is consistent with Muttoni et al. (2011) who also interpreted an unconformity at the base of the Sabbie di Imola where the Jaramillo normal chron was also missing at the Monte Poggiolo section, east our study area at the Panaro. The normal interval N4 in the Panaro section correlates to the 2n subchron between 1.78 and 1.99 Ma (Figure 6). Accordingly, magnetozone boundaries older than N4 are correlated to subsequent geomagnetic reversals because no other unconformities are observed in that part of the section. The final correlation shows the section spans the interval from 0.9 to 3.3 Ma (Figure 6). This correlation is consistent with the age determinations for the upper Argille Azzurre and Sabbie di Imola at the nearby Enza, Stirone, Arda, and Monte Poggiolo sections (Gunderson et al., 2012, 2014; Monesi et al., 2016; Muttoni et al., 2011).

3.2. Cyclostratigraphy

The χ data series can be roughly separated into two sections based on the χ amplitude (Figure 7 and Table S2 in the supporting information). Between ~0 and 200 m there is a very low amplitude variability in the χ data

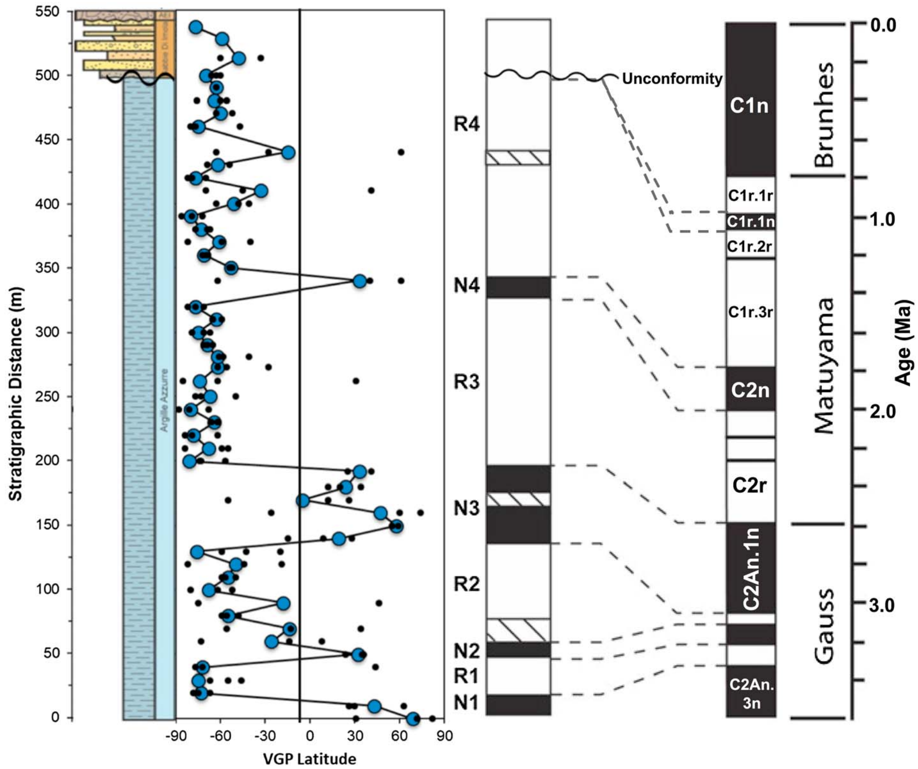

Figure 6. (a) Virtual geomagnetic pole (VGP) latitude of the Panaro samples. The blue circles represent the site mean VGP's, and the black circles represent the individual sample VGP's. Positive VGP's indicate a normal polarity and negative VGP's represent a reverse polarity. (b) Eight magnetozones are defined based on the mean VGP latitudes with white representing reversed polarity, black representing normal polarity, and dashed representing indeterminate polarity. The respective locations of the Sabbie di Imola and the unconformity at its base that helps us anchor the correlation are shown. (c) Correlation of magnetozones to the geomagnetic polarity timescale of Gradstein et al. (2012).

series. Between ~200 and 498 m, the χ data series shows large-amplitude variations that have several sharp peaks defined by a single sample, similar to what is observed in the nearby Stirone and Enza River sections (Gunderson et al., 2012, 2014). In order to investigate the χ data series for climate-related cyclicity, we performed multitaper method time series analysis. Before doing so, we rescaled the χ data series to absolute time using the Panaro magnetostratigraphy and resampled the data series at regular intervals. The resultant power spectrum shows broad peaks centered at frequencies of 1/512, 1/170, 1/44, and 1/20 kyr (Figure 8). The identification of significant obliquity (~40 kyr) and precession cycles (~20 kyr) encoded in the Argille Azzurre χ data series is consistent with the results from the Stirone and Enza river sections (Gunderson et al., 2012, 2014).

The Sabbie di Imola (~1.1–0.9 Ma) unit provides a time and rock-stratigraphic anchor that allows us to compare the new high-resolution age model for the Panaro section to the other growth sections exposed in the Stirone and Enza Rivers (Figure 9). The correlation between the three sections shows that the base of the Enza section only extends to 1.6 Ma, so we can compare deformation at all three structures only up to that point. From ~1.6 to 3.0 Ma, we have continuous records of deformation only at the Panaro and Stirone sections. Still, this provides sufficiently long, high-resolution records of fault-related folding to assess synchronous or asynchronous behavior in fault slip along strike.

3.3. Fault Slip Modeling

Figure 10 shows the best fit forward model results for the Enza and Panaro sections. The best fit models recreate the growth strata bedding dip measured at the surface for both sections within ±3°. In order to calculate the fault slip for dated horizons beyond the structural resolution of our forward models, we plotted the relationship between fault slip and bedding dip at the surface for our best fit models in Figure 11. We used the regression line for each structural model to transform measurements of bedding dip to fault slip for each horizon with geochronologic and surface structural control.

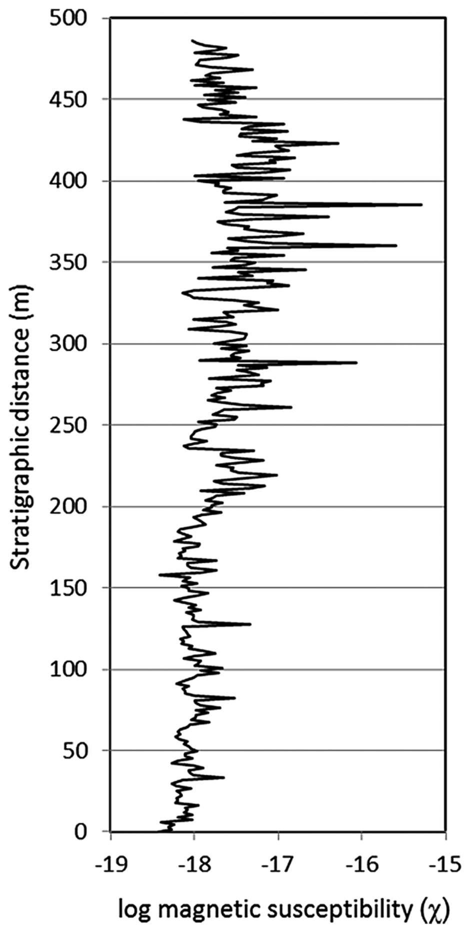

Figure 7. Magnetic susceptibility (χ) for the Argille Azzurre interval of the Panaro section.

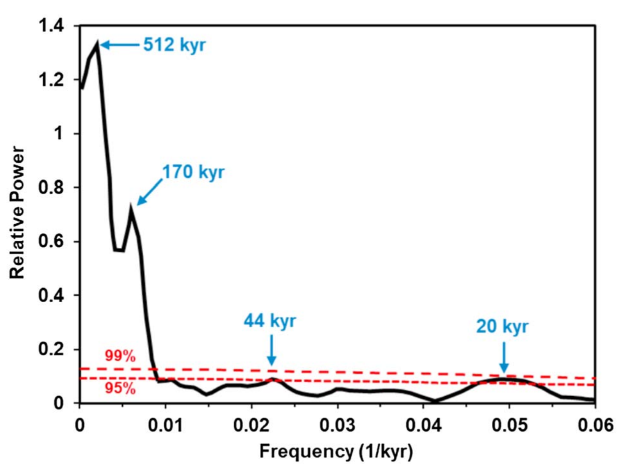

Figure 8. Multitaper method power spectrum for the Panaro section's untuned χ data series. The dashed red lines represent 95% and 99% confidence intervals above a robust red noise model. Significant spectral peaks are indicated.

Using the relationship between bedding dip and fault slip, we compiled slip histories for each of the three structures (Figure 12). Over the time span for which we had outcrop geochronologic control and were able model the deformation, the Salsomaggiore, Quattro Castella, and Castelvetro thrusts accumulated 1,549, 1,265, and 1,624 m of fault slip, respectively, which is equivalent to long-term average fault slip rates of 0.5, 0.8, and 0.5 mm/year. These long-term rates are consistent with fault slip rate calculations of similar blind thrusts in the Po Plain and Northern Apennines, which typically show long-term slip rates of <1.0 mm/year (Maesano et al., 2015).

The modeled slip histories demonstrate that slip accumulation was not constant through time (Figure 12). The slip histories show that the period between 1.0 and 3.0 Ma is generally characterized by relatively long and slow periods of fault slip and associated fold growth that is then punctuated by brief, rapid periods of folding and fault slip (Figure 12). Slip rates vary by 2 orders of magnitude, the lowest slip rate for a single 40-kyr time period measured for the Castelvetro thrust was <0.1 mm/year, and the greatest slip rate for a separate 40-kyr time period, for the same structure, was 3.4 mm/year.

These records of variable folding and faulting continue between 0 and 1.0 Ma, albeit at a reduced temporal resolution as recorded by the incised fluvial terraces, which also show variable incision (rock uplift) rates at each location (Figure 13). Although long-term fault slip rates and patterns of variability in the modeled slip histories at all three locations are similar, the specific timing of changes in slip rates are asynchronous between the structures from 1.0 to 3.0 Ma. After 1.0 Ma, the deformation rates change to become more synchronous (Figure 13).

4. Discussion

The high-resolution records of deformation observed in the growth strata and fluvial terraces provide insight into the variable slip behavior of the underlying faults deforming the northern Apennine mountain front. Although sharing some similarities in approach and in part inspired by a suite of related studies in central Asia (Charreau et al., 2005, 2006, 2008, 2009; Daëron et al., 2007), this study offers higher temporal resolution for fault-related deformational variability on adjacent structures over geologic time scales. The observation that each of these structures exhibits variable slip behavior over multiple time scales confirms predictions from numeric and analog models (Cowie et al., 1993; Naylor & Sinclair, 2007).

We interpret the asynchronous deformation observed at the three structural transects between 1.0 and 3.0 Ma as indicating that the variable fault slip behavior of the faults coring the mountain front folds is not controlled by extrinsic drivers, like a change in a tectonic boundary condition or variable surface loads. Additionally, the high-resolution deformational variability recorded by both the growth strata and terraces is not temporally coincident with orbitally driven climatic changes or variable sediment accumulation rates (Figure 12; Gunderson et al., 2014), suggesting that even local variations in erosion or deposition were not modulators of the slip rate variability on individual faults. Instead, we attribute the variable slip rate behavior to intrinsic forces such as cyclic strain hardening and softening or

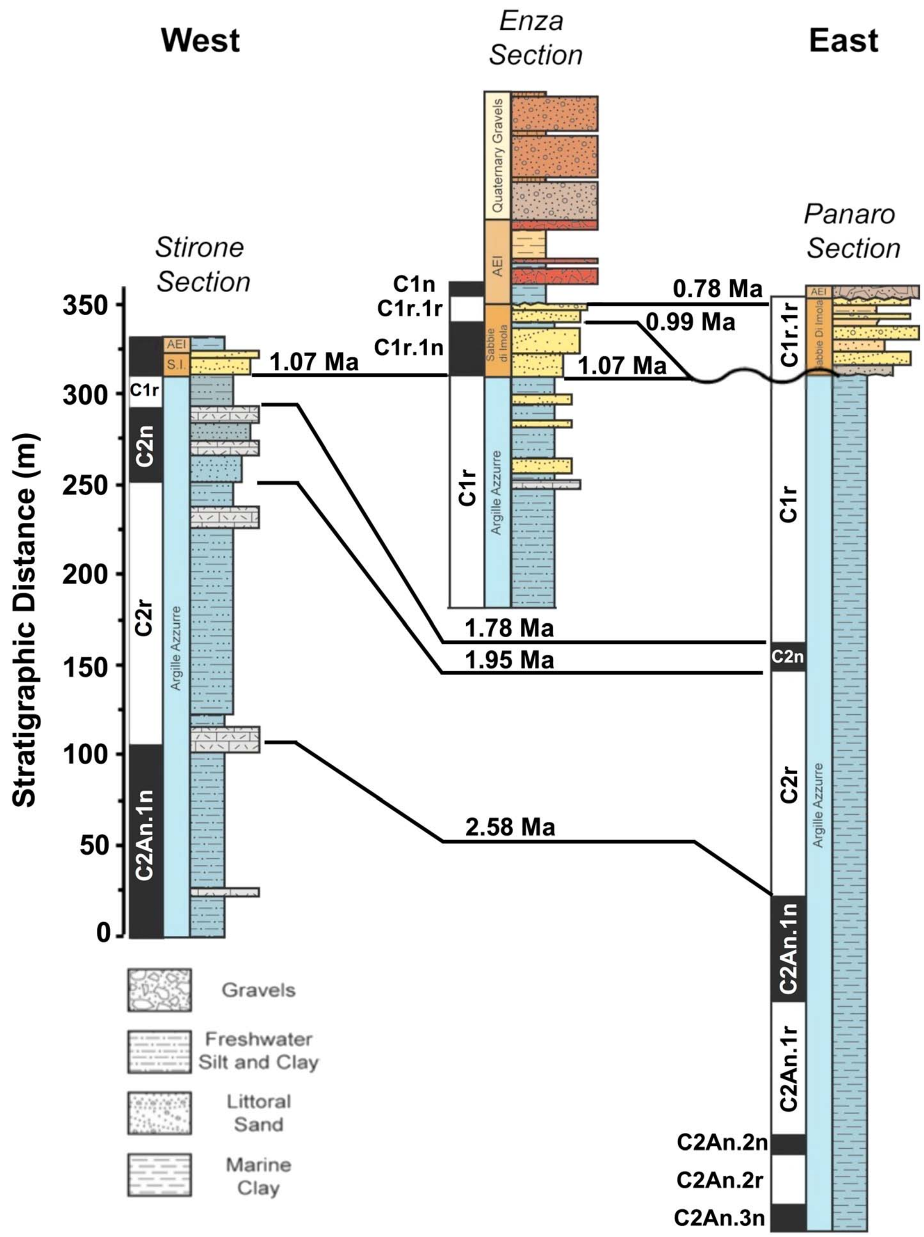

Figure 9. Correlation of the three growth sections using the age models developed for the Stirone (Gunderson et al., 2012), the Enza (Gunderson et al., 2014), and the Panaro (this study) sections.

slip being transferred to connected structures across strike, all processes that have been proposed for faults in other orogens (Roy et al., 2016).

There is a change, however, from clearly asynchronous to more synchronous variability after 1.0 Ma (Figure 13). This change temporally coincides with regional uplift of the modern-day mountain front thought to be linked to slip on the PTF, a proposed, deep, crustal-scale blind thrust fault (Boccaletti et al., 1985; Picotti & Pazzaglia, 2008; Figure 1). We suggest that the change to a more synchronous behavior and the subaerial emergence of the Northern Apennines in the last 1.0 Ma may be driven by the switch from variable slip of three disconnected, shallow thrusts, to slip on a basement-involved thick-skinned thrust that has a much longer strike length, spanning the entire northern Apennine mountain front. Not surprisingly, this proposed basement-involved thrust also exhibits variable slip behavior as manifest by the accelerations and decelerations in river incision over the last 1.0 Ma (Figure 13; Picotti & Pazzaglia, 2008; Wilson et al., 2009).

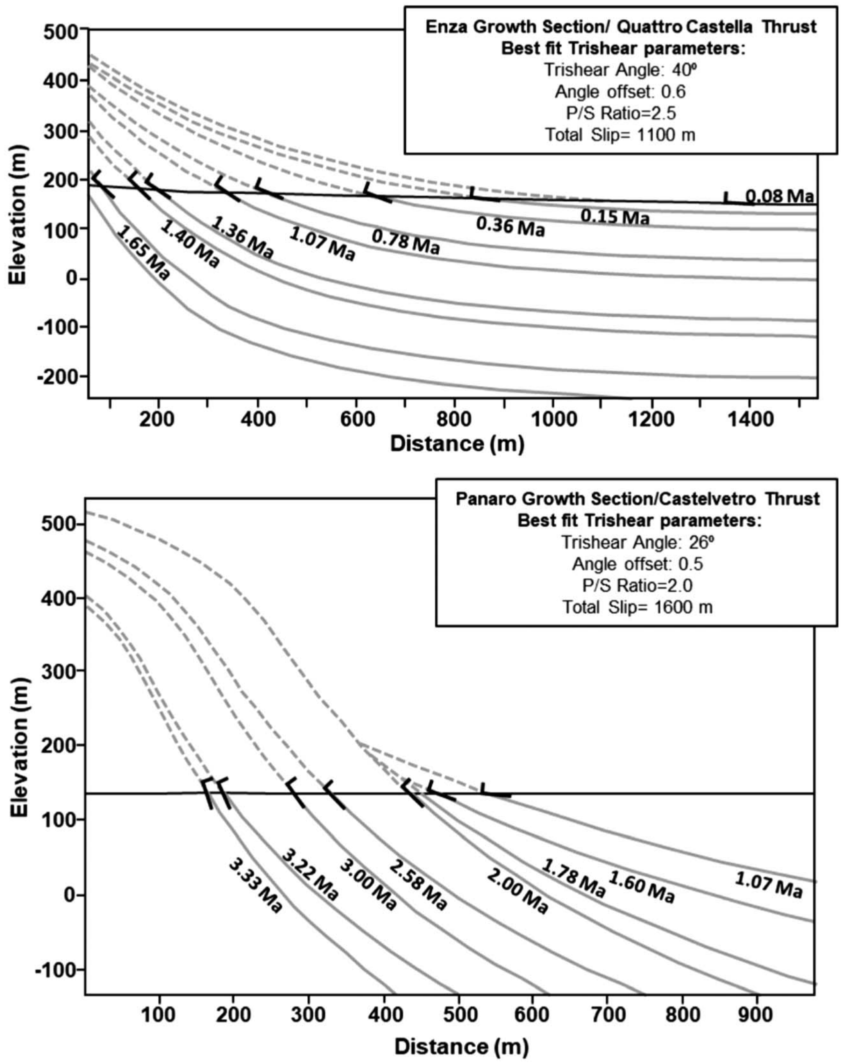

Figure 10. Best fit forward models of deformed growth strata for the Enza and Panaro transects (Figure 2). The geometry of the growth strata in these forward models matches those observed in subsurface seismic data and published cross sections (Figure 2; Oppo et al., 2013, 2015), and the surface bedding within ±3°. The surface bedding measurements are illustrated on the cross sections by surface dip markers.

The variable deformation histories documented for both the shallow blind thrust cored anticlines and the deep PTF is not surprising. At a first order, a fault-related fold with rotating limbs should exhibit variable deformation behavior over its active lifespan. This is because as rocks fold, planar anisotropies such as bedding and foliation tilt, varying the angle between the maximum compressive stress relative to layering through time. Since many rocks exhibit a parabolic yield curve, the relative orientation between stress axes and layering affects fracturing, faulting, and creep (Donath, 1961; Donath & Parker, 1964; Fisher, 1990; Paterson & Weiss, 1966). During folding, for example, strain softening is followed by strain hardening as limbs rotate and folds tighten.

The deformational variability observed on the faults in this study, however, goes beyond the first-order variability that is expected due to strain hardening in a tightening fold. Each of the structures in this study exhibits multiple periods of slip acceleration and deceleration that require further consideration. For example, our data are near the Apennine structural front where greater deformation heterogeneity is expected given the relatively low confining pressures on the blind faults (e.g., Handin & Hager, 1957). Furthermore, fluid, mechanical, and fault slip processes all lead to deformation rate variability (Biemiller & Lavier, 2017; Saffer & Tobin, 2011), but determining one specific control on slip rate variability is difficult, as the evidence for specific processes controlling fault slip rates can be ambiguous. With this in mind, we discuss the following

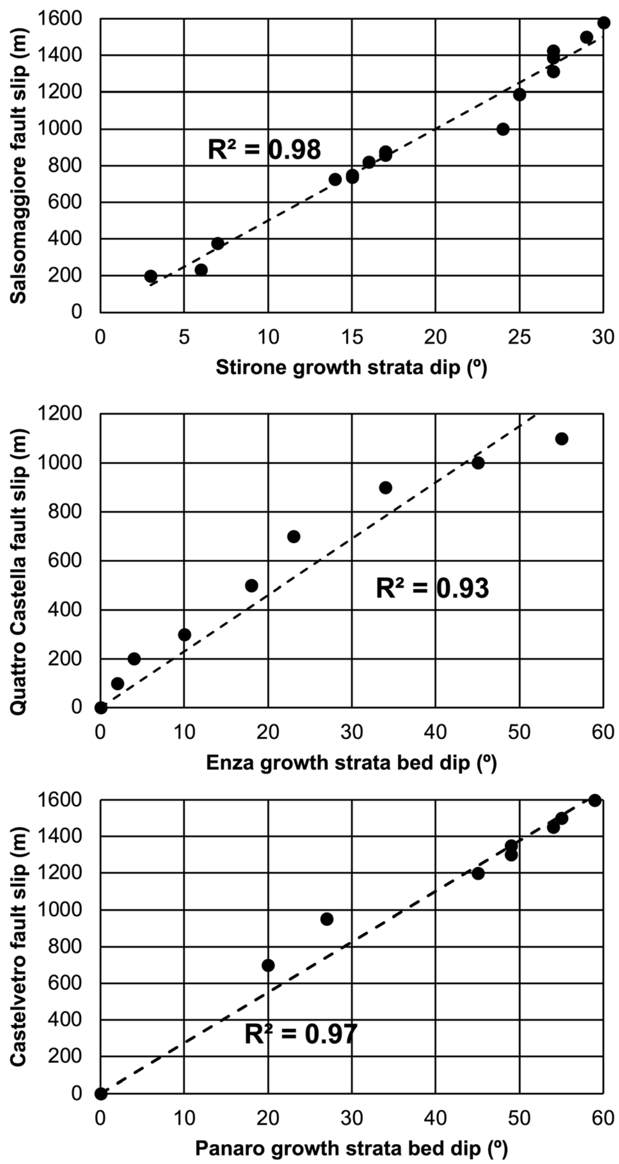

Figure 11. Graphs showing the correlation between growth strata bedding dip measured at the surface and the modeled fault slip for the Salsomaggiore (from Gunderson et al., 2013), Quattro Castella (this study), and Castelvetro thrusts (this study). This correlation allows us to compute fault slip for horizons for which we have surface measurements of bedding dip and chronologic control but are too closely spaced to correlate into the subsurface because that tight spacing is beyond the resolution afforded by subsurface seismic and our structural cross sections.

processes as potential intrinsic controls on fault slip rate variability for faults in this study. These include the following: (1) changes in fault strength due to temporally variable pore pressure (e.g., Krueger & Grant, 2011), (2) strain partitioning on adjacent connected faults (e.g., Bennett et al., 2004), and (3) lateral fault propagation and linkage with adjacent faults (e.g., McCartney & Scholz, 2016).

Because of the strong impact of pore pressure on fault strength (Hubbert & Rubey, 1959), variations in the pore pressure regime will lead to coordinated transience on slip events (Gretner, 1981). Subsurface pore pressure changes can be caused by intrinsic processes and do not necessitate external forcing. For instance, as slip accumulates on a fault, the porosity and permeability of the fault zone can either increase or decrease, depending on the lithology of the fault's host rock (Antonellini & Aydin, 1994). This change in fault zone permeability can affect the pore pressure environment by allowing the fault to become a conduit for fluids or to create a barrier for overpressure dissipation. The fault-related folds at the northern Apennine mountain front are cored by Miocene turbidite sandstones, which means that the thrust faults in the sandstones likely deform by cataclasis, a process that decreases fault zone porosity and permeability through time and thereby has the potential to influence pore pressure heterogeneity. Another possibility is that the natural pore pressure evolution of buried ramp thrusts leads to deformation variability. This was demonstrated by Krueger and Grant (2011) for similar tip-line folds in the Niger Delta toe-thrust belt. There it was demonstrated that as porous sandstones are progressively buried and continuously deform, a significant pressure differential builds up between the downdip backlimb syncline and the anticlinal crest, which leads to the transfer of high pore pressures updip. This pressure transfer weakens the fault zones and initiates slip failure. In the Niger Delta example, episodic pore pressure increases directly relate to periods of episodic accelerated deformation (Krueger & Grant, 2011). The presence of mud volcanoes and fluid expulsion chimneys over the crests of the Salsomaggiore, Quattro Castella, and Castelvetro anticlines (Bonini, 2007; Oppo et al., 2015) is direct evidence that significant overpressure developed in these northern Apennine structures. It is a strong possibility that variability in the pressure regime through time could be the intrinsic control on the observed slip rate variability.

Another possibility is that the variable slip behavior on individual faults in the Northern Apennines is a product of slip partitioning on connected thrusts. At much lower temporal resolution, Maesano et al. (2015) documented across-strike slip partitioning on similar blind thrust faults east of our study area in the Ferrara and Romagna Apennine thrust fronts. Similarly, correlation of the growth strata on the forelimb of the Salsomaggiore anticline onto the backlimb of the buried, foreland Cortemaggiore anticline (Figure 2) suggests that the Cortemaggiore thrust and the Salsomaggiore thrust were active contemporaneously and that Cortemaggiore was active during Salsomaggiore's long period of quiescence between 2.0 and 2.6 Ma (Artoni et al., 2007). Since these faults share a common detachment, it is possible that regional shortening rates could have remained constant over the period of time these thrusts were active, but where the bulk of the shortening was accommodated alternated between the two structures. Unfortunately, because the Cortemaggiore anticline is currently buried under the Po Plain, there is no surface exposure of growth strata that we can use to determine a high-resolution slip history, and the resolution afforded by seismic correlation does not allow us to compare the deformational history of Salsomaggiore and Cortemaggiore at the same temporal scale.

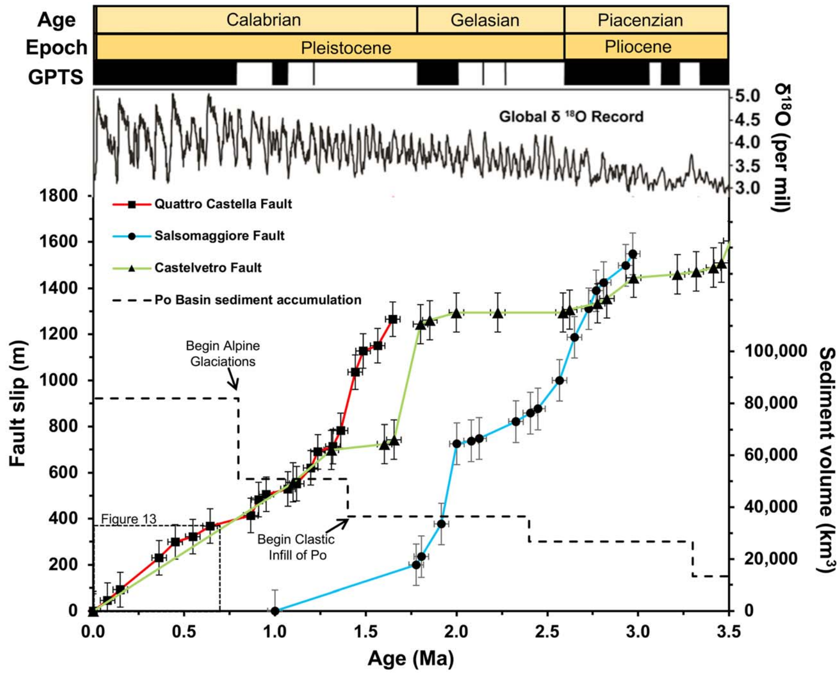

Figure 12. Fault slip histories for the Salsomaggiore thrust (blue), Quattro Castella thrust (red), and the Castelvetro thrust (green). Each point in the slip history represents a measurable change in bedding dip at the surface that we inverted for fault slip using the calculated bedding-fault slip relationship in Figure 11 that was generated from our forward models. The sedimentation history for the Po Plain (from Ghielmi et al., 2010) is represented by the black dashed line. The high-frequency deformation variability observed in the slip histories is asynchronous and not correlated to high-frequency climatic changes (solid black line- δ^{18}O from Lisiecki & Raymo, 2005), suggesting that the driving force of this variability is not an extrinsic boundary condition change to the Apennine orogenic wedge. See text for further interpretation.

We recognize that the slip histories we compiled in Figure 12 represent an incomplete view of the slip behavior of the entire thrust sheet because we calculate slip histories from a single transect for each fault. As faults grow and propagate laterally, there is a gradient in displacement along strike for each slip event, with a maximum displacement at the fault center that decreases toward the fault tips (Walsh & Watterson, 1989). Lateral fault growth and linkage can cause the illusion of unsteady slip behavior if the slip history is measured at a location that was once near the tip of a propagating fault that later linked with another structure to create a larger composite fault (Bergen et al., 2017; McCartney & Scholz, 2016; Mueller, 2017). However, this is an unlikely explanation for the variable slip behavior compiled for at least two of the three structures in this study. The growth sections that record the slip history for the Salsomaggiore and Quattro Castella faults are located near lateral ramps close to the eastern ends of relatively large thrust sheets. Regional cross sections do not provide strong evidence that these faults grew through significant linkage during the time span studied here (Oppo et al., 2013). Only the Castelvetro thrust (Panaro section) may be partially influenced by fault growth and linkage effects. Regional cross sections show that the thrust faults underlying the Apennine mountain front in that area tend to be smaller in length but linked (Maesano et al., 2015; Oppo et al., 2013); therefore, it is possible that a complex history of fault growth and linkage could explain the variable slip behavior there.

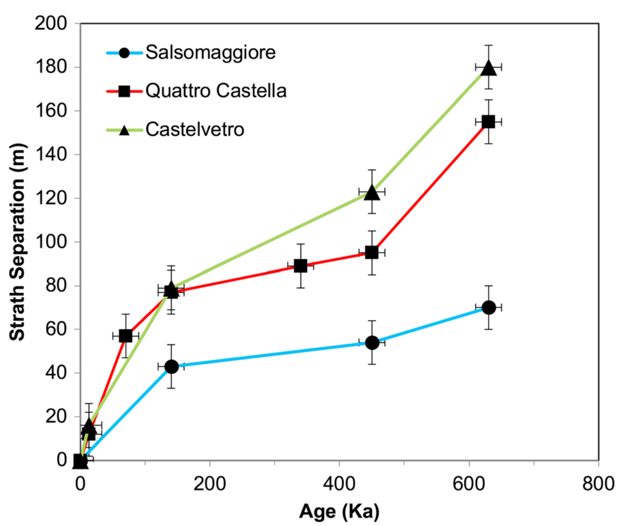

Figure 13. River incision for the Stirone (blue; Wilson et al., 2009), Enza (red; Ponza et al., 2010); and Panaro Rivers (green; Ponza et al., 2010). Inasmuch as incision rates are a proxy for uplift rates, they show synchronous uplift at all three transects. The change from asynchronous to synchronous uplift is related to the activation of an orogen-scale thick-skinned thrust between 1.0–1.4 Ma that is responsible for most of the recent deformation of the Apennine mountain front.

A question that remains unanswered is why, at the locations of this study, there was a change in deformation character in the Apennine orogen from slip primarily focused on shallow imbricate thrusts of limited strike lengths to a basement-involved thrust spanning the length of the mountain front at ~1.0 Ma. We see two possible explanations for this change. The first explanation is to note that the transition from thin-skinned to thick-skinned deformation at the modern-day mountain front between ~1.0 and 1.4 Ma is coincident with a wedge boundary condition change that resulted in the overfilling of the Po foreland and the reduction of the orogenic wedge's critical taper (Figure 12). This suggests that surface processes and load redistribution, as an extrinsic driver, might control the locus and rates of deformation on faults in an orogenic wedge but at only longer spatial (greater than hundreds of kilometers) and temporal ($>10^6$ years) scales (Hetzel & Hampel, 2005). This explanation is supported by the documented deceleration in deformation that has occurred on the frontal thrusts of the Emilia and Ferrara arcs buried in the Po Plain (Maesano et al., 2015) and the large influx of sediment deposited on the toe of wedge in the last 1.4 Ma (Figure 12).

Another explanation for this switch is that basement-involved deformation of the wedge has always been occurring, but when the shallow thrusts in this study were most active, the basement-involved deformation occurred at a more hinterland location and its effects were not recorded by the growth strata in the Stirone, Enza, or Panaro sections. This explanation implies that when the syntectonic sedimentary records show a switch from "thin-skinned" to "thick-skinned" deformation, they are illustrating the foreland propagation of the thick-skinned portion of the orogenic wedge and the associated mountain front monocline (i.e., Vann et al., 1986). This explanation can also account for the apparent slowing of the thin-skinned thrust sheets in the Po foreland, since we have already demonstrated that these structures exhibit deformational rate variability over a range of time scales. It is possible that the apparent deceleration we observe on these structures over the past 1.0 Ma is simply biased by length of record and that the shallow, disconnected thrust faults will accelerate again in the future.

5. Conclusions

We have compiled a novel data set that reveals the underlying slip behavior of three disconnected faults coring actively growing folds along strike at the modern-day northern Apennine mountain front. We show that the faults exhibit variable slip behavior over a 3.0-Myr time period and demonstrate that for most of the time, this variable slip behavior is asynchronous for the different structures along strike, suggesting that the high-frequency deformation variability is not driven by an extrinsic boundary condition change. We conclude that the variability observed on these temporal and spatial scales is consistent with the natural, intrinsic behavior of faults in an orogenic wedge at intermediate time and space scales, and not caused by extrinsic drivers such as tectonic boundary condition or climatic changes.

Acknowledgments
We thank C. Berti, A. Teletzke, and A. Ponza for help with data collection. D. Minguez and V. Picotti provided helpful feedback regarding the paleomagnetic results and Apennine geology. This manuscript was improved due to helpful reviews by S. Satolli and R. Gold in addition to the feedback from the Editors. This work was supported by the National Science Foundation (EAR-0809722) and by graduate research grants from the American Association of Petroleum Geologists and the Geological Society of America. Data from this study can be found in Tables S1 and S2 in the supporting information.

References

Allmendinger, R. W. (1998). Inverse and forward numerical modeling of trishear fault-propagation folds. *Tectonics*, *17*(4), 640–656. https://doi.org/10.1029/98TC01907

Amorosi, A., & Pavesi, M. (2010). Aquifer stratigraphy from the middle-late Pleistocene succession of the Po Basin. *Memorie Descrittive Della Carta Geologica d'Italia*, *90*, 7–20.

Antonellini, M., & Aydin, A. (1994). Effect of faulting on fluid flow in porous sandstones: Petrophysical properties. *AAPG Bulletin*, *78*(3), 355–377.

Argnani, A., Barbacini, G., Bernini, M., Camurri, F., Ghielmi, M., Papani, G., et al. (2003). Gravity tectonics driven by Quaternary uplift in the Northern Apennines; insights from the La Spezia-Reggio Emilia geo-transect. *Quaternary International*, *101-102*, 13–26. https://doi.org/10.1016/S1040-6182(02)00088-5

Artoni, A., Papani, G., Rizzini, F., Calderoni, M., Bernini, M., Argnani, A., et al. (2004). The Salsomaggiore structure (northwestern Apennine foothills, Italy): A Messinian mountain front shaped by mass-wasting products. *GeoActa (Bologna)*, *3*, 107–127.

Artoni, A., Rizzini, F., Roveri, M., Gennari, R., Manzi, V., Papani, G., & Bernini, M. (2007). Tectonic and climatic controls on sedimentation in late Miocene Cortemaggiore wedge-top basin (northwestern Apennines, Italy). In *Thrust belts and foreland basins* (pp. 431–456). Berlin: Springer. https://doi.org/10.1007/978-3-540-69426-7_23

Basili, R., & Barba, S. (2007). Migration and shortening rates in the Northern Apennines, Italy: Implications for seismic hazard. *Terra Nova*, *19*(6), 462–468. https://doi.org/10.1111/j.1365-3121.2007.00772.x

Bennett, R. A., Friedrich, A. M., & Furlong, K. P. (2004). Codependent histories of the San Andreas and San Jacinto fault zones from inversion of fault displacement rates. *Geology*, *32*(11), 961–964. https://doi.org/10.1130/G20806.1

Bennett, R. A., Serpelloni, E., Hreinsdottir, S., Brandon, M. T., Buble, G., Basic, T., et al. (2012). Syn-convergent extension observed using the RETREAT GPS network, Northern Apennines, Italy. *Journal of Geophysical Research*, *117*, B04408. https://doi.org/10.1029/2011JB008744

Benoit, M. H., Torpey, M., Liszewski, K., Levin, V., & Park, J. (2011). *P* and *S* wave upper mantle seismic velocity structure beneath the Northern Apennines: New evidence for the end of subduction. *Geochemistry, Geophysics, Geosystems*, *12*, Q06004. https://doi.org/10.1029/2010GC003428

Bergen, K. J., Shaw, J. H., Leon, L. A., Dolan, J. F., Pratt, T. L., Ponti, D. J., et al. (2017). Accelerating slip rates on the Puente Hills blind thrust fault system beneath metropolitan Los Angeles, California, USA. *Geology*, *45*(3), 227–230. https://doi.org/10.1130/G38520.1

Biemiller, J., & Lavier, L. (2017). Earthquake supercycles as part of a spectrum of normal fault cycles. *Journal of Geophysical Research: Solid Earth*, *122*, 3221–3240. https://doi.org/10.1002/2016JB013666

Boccaletti, M., Coli, M., Eva, C., Ferrari, G., Giglia, G., Lazzarotto, A., et al. (1985). Considerations on the seismotectonics of the Northern Apennines. *Tectonophysics*, *117*(1-2), 7–38. https://doi.org/10.1016/0040-1951(85)90234-3

Bonini, M. (2007). Interrelations of mud volcanism, fluid venting, and thrust-anticline folding: Examples from the external Northern Apennines (Emilia-Romagna, Italy). *Journal of Geophysical Research*, *112*, B08413. https://doi.org/10.1029/2006JB004859

Brodsky, E. E., Roeloffs, E., Woodcock, D., Gall, I., & Manga, M. (2003). A mechanism for sustained groundwater pressure changes induced by distant earthquakes. *Journal of Geophysical Research*, *108*(B8), 2390. https://doi.org/10.1029/2002JB002321

Carminati, E., & Doglioni, C. (2012). Alps vs. Apennines: The paradigm of a tectonically asymmetric earth. *Earth-Science Reviews*, *112*(1-2), 67–96. https://doi.org/10.1016/j.earscirev.2012.02.004

Cavinato, G. P., & De Celles, P. G. (1999). Extensional basins in the tectonically bimodal central Apennines fold-thrust belt, Italy: Response to corner flow above a subducting slab in retrograde motion. *Geology*, *27*(10), 955–958. https://doi.org/10.1130/0091-7613(1999)027<0955:EBITTB>2.3.CO;2

Charreau, J., Avouac, J.-P., Chen, Y., Dominguez, S., & Gilder, S. (2008). Miocene to present kinematics of fault-bend folding across the Huerguosi anticline, northern Tianshan (China), derived from structural, seismic, and magnetostratigraphic data. *Geology*, *36*(11), 871–874 . https://doi.org/10.1130/G25073A.1

Charreau, J., Chen, Y., Gilder, S., Barrier, L., Dominguez, S., Augier, R., et al. (2009). Neogene uplift of the Tian Shan Mountains observed in the magnetic record of the Jingou River section (northwest China). *Tectonics*, *28*, TC2008. https://doi.org/10.1029/2007TC002137

Charreau, J., Chen, Y., Gilder, S., Dominguez, S., Avouac, J.-P., Sen, S., et al. (2005). Magnetostratigraphy and rock magnetism of the Neogene Kuitun He section (northwest China): Implications for Late Cenozoic uplift of the Tianshan mountains. *Earth and Planetary Science Letters*, *230*(1-2), 177–192. https://doi.org/10.1016/j.epsl.2004.11.002

Charreau, J., Gilder, S., Chen, Y., Dominguez, S., Avouac, J.-P., Sen, S., et al. (2006). Magnetostratigraphy of the Yaha section, Tarin Basin (China): 11 Ma acceleration in erosion and uplift of the Tian Shan mountains. *Geology*, *34*(3), 181–184. https://doi.org/10.1130/G22106.1

Chéry, J., & Vernant, P. (2006). Lithospheric elasticity promotes episodic fault activity. *Earth and Planetary Science Letters*, *243*(1-2), 211–217. https://doi.org/10.1016/j.epsl.2005.12.014

Cowie, P. A., Roberts, G. P., Bull, J. M., & Visini, F. (2012). Relationships between fault geometry, slip rate variability and earthquake recurrence in extensional settings. *Geophysical Journal International*, *189*(1), 143–160. https://doi.org/10.1111/j.1365-246X.2012.05378.x

Cowie, P. A., Vanneste, C., & Sornette, D. (1993). Statistical physics model for the spatio-temporal evolution of faults. *Journal of Geophysical Research*, *98*, 21,809–21,822.

Daëron, M., Avouac, J.-P., & Charreau, J. (2007). Modeling the shortening history of a fault tip using structural and geomorphic records of deformation. *Journal of Geophysical Research*, *112*, B03S13. https://doi.org/10.1029/2006JB004460

Davis, J. L., Wernicke, B. P., Bisnath, S., Niemi, N. A., & Elósegui, P. (2006). Subcontinental-scale crustal velocity changes along the Pacific–North America plate boundary. *Nature*, *441*(7097), 1131–1134. https://doi.org/10.1038/nature04781

Dolan, J. F., & Haravitch, B. D. (2014). How well do surface slip measurements track slip at depth in large strike-slip earthquakes? The importance of fault structural maturity in controlling on-fault slip verses off-fault surface deformation. *Earth and Planetary Science Letters*, *388*, 38–47. https://doi.org/10.1016/j.epsl.2013.11.043

Dolan, J. F., McAuliffe, L. J., Rhodes, E. J., McGill, S. F., & Zinke, R. (2016). Extreme multi-millennial slip rate variations on the Garlock fault, California: Strain super-cycles, potentially time-variable fault strength, and implications for system-level earthquake occurrence. *Earth and Planetary Science Letters*, *446*, 123–136. https://doi.org/10.1016/j.epsl.2016.04.011

Dolan, J. F., & Meade, B. J. (2017). A comparison of geodetic and geologic rates prior to large strike-slip earthquakes: A diversity of earthquake-cycle behaviors? *Geochemistry, Geophysics, Geosystems*, *18*, 4426–4436. https://doi.org/10.1002/2017GC007014

Donath, F. A. (1961). Experimental study of shear failure in anisotropic rocks. *Geological Society of America Bulletin*, *72*(6), 985–989. https://doi.org/10.1130/0016-7606(1961)72[985:ESOSFI]2.0.CO;2

Donath, F. A., & Parker, R. B. (1964). Folds and folding. *Geological Society of America Bulletin*, *75*(1), 45–62. https://doi.org/10.1130/0016-7606(1964)75[45:FAF]2.0.CO;2

Erslev, E. A. (1991). Trishear fault-propagation folding. *Geology*, *19*(6), 617–620. https://doi.org/10.1130/0091-7613(1991)019<0617:TFPF>2.3.CO;2

Fisher, D. M. (1990). Orientation history and rheology in slates, Kodiak and Afognak Islands, Alaska. *Journal of Structural Geology*, *12*(4), 483–498. https://doi.org/10.1016/0191-8141(90)90036-X

Fisher, R. A. (1953). Introductions to statistical methods applied to directional data. *Proceedings of the Royal Society of London*, *A217*, 295–305.

Friedrich, A. M., Wernicke, B. P., Niemi, N. A., Bennett, R. A., & Davis, J. L. (2003). Comparison of geodetic and geologic data from the Wasatch region, Utah, and implications for the spectral character of Earth deformation at periods of 10 to 10 million years. *Journal of Geophysical Research*, *108*(B4), 2199. https://doi.org/10.1029/2001JB000682

Ghielmi, M., Minervini, M., Nini, C., Rogledi, S., Rossi, M., & Vignolo, A. (2010). Sedimentary and tectonic evolution in the eastern Po-Plain and northern Adriatic Sea area from Messinian to Middle Pleistocene (Italy). *Rendiconti Accademia Fisiche Lincei*, *21*, S131–S166.

Ghil, M., Allen, M. R., Dettinger, M. D., Ide, K., Kondrashov, D., Mann, M. E., et al. (2002). Advanced spectral methods for climatic time series. *Reviews of Geophysics*, *40*(1), 1003. https://doi.org/10.1029/2000RG000092

Gold, R. D., & Cowgill, E. (2011). Deriving fault-slip histories to test for secular variation in slip, with examples from the Kunlun and Awatere faults. *Earth and Planetary Science Letters*, *301*(1-2), 52–64. https://doi.org/10.1016/j.epsl.2010.10.011

Gold, R. D., Cowgill, E., Arrowsmith, J. R., & Friedrich, A. M. (2017). Pulsed strain release on the Altyn Tagh fault, northwest China. *Earth and Planetary Science Letters*, *459*, 291–300. https://doi.org/10.1016/j.epsl.2016.11.024

Gradstein, F. M., Ogg, J. G., Schmitz, M. D., & Ogg, G. M. (2012). *The geologic time scale 2013* (1176 pp.). Netherlands, Amsterdam: Elsevier. https://doi.org/10.1016/B978-0-444-59425-9.01001-5

Gretner, P. E. (1981). Pore pressure, discontinuities, isostasy and overthrusts. *Geological Society of London, Special Publication*, *9*(1), 33–39. https://doi.org/10.1144/GSL.SP.1981.009.01.04

Gunderson, K. L., Anastasio, D. J., Pazzaglia, F. J., & Picotti, V. (2013). Fault slip rate variability on 10^4–10^5 yr timescales for the Salsomaggiore blind thrust fault, Northern Apennines, Italy. *Tectonophysics*, *608*, 356–365. https://doi.org/10.1016/j.tecto.2013.09.018

Gunderson, K. L., Kodama, K. P., Anastasio, D. J., & Pazzaglia, F. J. (2012). Rock-magnetic cyclostratigraphy for the late Pliocene-early Pleistocene Stirone section, Northern Apennine mountain front, Italy. *Geological Society Special Publication*, *373*, 16. https://doi.org/10.1144/SP373.8

Gunderson, K. L., Pazzaglia, F. J., Picotti, V., Anastasio, D. A., Kodama, K. P., Rittenour, T., et al. (2014). Unraveling tectonic and climatic controls on synorogenic growth strata (Northern Apennines, Italy). *Geological Society of America Bulletin*, *126*(3-4), 532–552. https://doi.org/10.1130/B30902.1

Hampel, A., Hetzel, R., & Maniatis, G. (2010). Response of faults to climate-driven changes in ice and water volumes on Earth's surface. *Philosophical Transactions of the Royal Society A*, *368*(1919), 2501–2517. https://doi.org/10.1098/rsta.2010.0031

Handin, J., & Hager, R. V. Jr. (1957). Experimental deformation of sedimentary rocks under confining pressure: Tests at room temperature on dry samples. *American Association of Petroleum Geologists Bulletin*, *41*, 1–50.

Hetzel, R., & Hampel, A. (2005). Slip rate variations on normal faults during glacial-interglacial changes in surface loads. *Nature*, *435*(7038), 81–84. https://doi.org/10.1038/nature03562

Hubbert, M. K., & Rubey, W. W. (1959). Role of fluid pressure in mechanics of overthrust faulting: I. Mechanics of fluid-filled porous solids and its application to overthrust faulting. *Geological Society of America Bulletin*, *70*(2), 115–166. https://doi.org/10.1130/0016-7606(1959)70[115:ROFPIM]2.0.CO;2

Kirschvink, J. (1980). The least-squares line and plane and the analysis of paleomagnetic data. *Geophysical Journal Royal Astronomical Society*, *62*(3), 699–718. https://doi.org/10.1111/j.1365-246X.1980.tb02601.x

Krueger, S. W., & Grant, N. T. (2011). The growth history of toe thrusts of the Niger Delta and the role of pore pressure. In K. McClay, J. H. Shaw, & J. Suppe (Eds.), *Thrust-fault related folding, American Association of Petroleum Geologists memoir 94* (pp. 357–390).

Langer, J. S., Carlson, J. M., Myers, C. R., & Shaw, B. E. (1996). Slip complexity in dynamic models of earthquake faults. *Proceedings of the National Academy of Sciences, United States of America*, *93*, 3825–3829.

Laskar, J., Robutel, P., Joutel, F., Gastineau, M., Correia, A. C. M., & Levrard, B. (2004). A long-term numerical solution for the insolation quantities of the Earth. *Astronomy and Astrophysics*, *428*(1), 261–285. https://doi.org/10.1051/0004-6361:20041335

Lavé, J., & Avouac, J. P. (2001). Fluvial incision and tectonic uplift across the Himalayas of central Nepal. *Journal of Geophysical Research*, *106*(B11), 26,561–26,591. https://doi.org/10.1029/2001JB000359

Lisiecki, L. E., & Raymo, M. E. (2005). A Pliocene-Pleistocene stack of 57 globally disturbed benthic delta (super 18) O records. *Paleoceanography*, *20*, PA1003. https://doi.org/10.1029/2004PA001071

Lowry, A. R. (2006). Resonant slow fault slip in subduction zones forced by climatic load stress. *Nature*, *442*(7104), 802–805. https://doi.org/10.1038/nature05055

Maesano, F. E., D'Ambrogi, C., Burrato, P., & Toscani, G. (2015). Slip-rates of blind thrusts in slow deforming areas: Examples from the Po Plain (Italy). *Tectonophysics*, *643*, 8–25. https://doi.org/10.1016/j.tecto.2014.12.007

Mann, M. E., & Lees, J. M. (1996). Robust estimation of background noise and signal detection in climatic time series. *Climatic Change*, *33*(3), 409–445. https://doi.org/10.1007/BF00142586

Mary, C., Iaccarino, S., Courtillot, V., Besse, J., & Aissaoui, D. M. (1993). Magnetostratigraphy of Pliocene sediments from the Stirone River (Po valley). *Geophysical Journal International*, *112*(3), 359–380. https://doi.org/10.1111/j.1365-246X.1993.tb01175.x

McCartney, T., & Scholz, C. A. (2016). A 1.3 million year record of synchronous faulting in the hangingwall and border fault of a half-graben in the Malawi (Nyasa) Rift. *Journal of Structural Geology*, *91*, 114–129. https://doi.org/10.1016/j.jsg.2016.08.012

Monesi, E., Muttoni, G., Scardia, G., Felletti, F., Bona, F., Sala, B., et al. (2016). Insights on the opening of the Galerian mammal migration pathway from magnetostratigraphy of the Pleistocene marine–continental transition in the Arda River section (northern Italy). *Quaternary Research*, *86*(02), 220–231. https://doi.org/10.1016/j.yqres.2016.07.006

Mouslopoulou, V., Walsh, J. J., & Nicol, A. (2009). Fault displacement rates on a range of timescales. *Earth and Planetary Science Letters*, *278*(3-4), 186–197. https://doi.org/10.1016/j.epsl.2008.11.031

Mueller, K. (2017). Variation in slip rates on active faults: Natural growth or stress transients? *Geology*, *45*(3), 287–288. https://doi.org/10.1130/focus032017.1

Muttoni, G., Scardia, G., Kent, D. V., Morsiani, E., Tremolada, F., Cremaschi, M., & Peretto, C. (2011). First dated human occupation of Italy at ~0.85 Ma during the late Early Pleistocene climate transition. *Earth and Planetary Science Letters*, *307*(3-4), 241–252. https://doi.org/10.1016/j.epsl.2011.05.025

Naylor, M., & Sinclair, H. (2007). Punctuated thrust deformation in the context of doubly vergent thrust wedges: Implications for the localization of uplift and exhumation. *Geology*, *35*(6), 559–562. https://doi.org/10.1130/G23448A.1

Oakley, D. O. S., & Fisher, D. M. (2015). Inverse trishear modeling of bedding dip data using Markov chain Monte Carlo methods. *Journal of Structural Geology*, *80*, 157–172. https://doi.org/10.1016/j.jsg.2015.09.005

Oppo, D., Capozzi, R., & Picotti, V. (2013). A new model of the petroleum system in the Northern Apennines, Italy. *Marine and Petroleum Geology*, *48*, 57–76. https://doi.org/10.1016/j.marpetgeo.2013.06.005

Oppo, D., Capozzi, R., Picotti, V., & Ponza, A. (2015). A genetic model of hydrocarbon-derived carbonate chimneys in shelfal fine-grained sediments: The Enza River field, Northern Apennines (Italy). *Marine and Petroleum Geology*, *66*, 555–565. https://doi.org/10.1016/j.marpetgeo.2015.03.002

Paterson, M. S., & Weiss, L. E. (1966). Experimental deformation and folding in phyllite. *Geological Society of America Bulletin*, *77*(4), 343–374. https://doi.org/10.1130/0016-7606(1966)77[343:EDAFIP]2.0.CO;2

Picotti, V., & Pazzaglia, F. J. (2008). A new active tectonic model for the construction of the Northern Apennines mountain front near Bologna (Italy). *Journal of Geophysical Research*, *113*, B08412. https://doi.org/10.1029/2007JB005307

Pollitz, F. F., Bürgmann, R., & Segall, P. (1998). Joint estimation of afterslip rate and postseismic relaxation following the 1989 Loma Prieta earthquake. *Journal of Geophysical Research*, *103*, 69–75.

Pondrelli, S., Salimbeni, S., Ekstrom, G., Morelli, A., Gasperini, P., & Vannucci, G. (2006). The Italian CMT dataset from 1977 to the present. *Physics of the Earth and Planetary Interiors*, *159*(3-4), 286–303. https://doi.org/10.1016/j.pepi.2006.07.008

Ponza, A., Pazzaglia, F. J., & Picotti, V. (2010). Thrust-fold activity at the mountain front of the Northern Apennines (Italy) from quantitative landscape analysis. *Geomorphology*, *123*(3-4), 211–231. https://doi.org/10.1016/j.geomorph.2010.06.008

Ricci Lucchi, F. (1986). The Oligocene to recent foreland basins of the Northern Apennines. *Special Publication of the International Association of Sedimentologists*, *8*, 105–139.

Rogers, G., & Dragert, H. (2003). Episodic tremor and slip on the Cascadia subduction zone: The chatter of silent slip. *Science*, *300*(5627), 1942–1943. https://doi.org/10.1126/science.1084783

Roy, S. G., Koons, P. O., Upton, P., & Tucker, G. E. (2016). Dynamic links among rock damage, erosion, and strain during orogenesis. *Geology*, *44*(7), 583–586. https://doi.org/10.1130/G37753.1

Saffer, D. M., & Tobin, H. J. (2011). Hydrology and mechanics of subduction zone forearcs: Fluid flow and pore pressure. *Annual Reviews of Earth and Planetary Sciences*, *39*(1), 157–186. https://doi.org/10.1146/annurev-earth-040610-133408

Sagnotti, L., & Winkler, A. (1999). Rock magnetism and palaeomagnetism of greigite-bearing mudstones in the Italian peninsula. *Earth and Planetary Science Letters*, *165*(1), 67–80. https://doi.org/10.1016/S0012-821X(98)00248-9
Saint-Carlier, D., Charreau, J., Lave, J., Blard, P.-H., Dominguez, S., Avouac, J.-P., et al. (2016). Major temporal variations in shortening rate absorbed along a large active fold of the southeastern Tianshan piedmont (China). *Earth and Planetary Science Letters*, *434*, 333–348. https://doi.org/10.1016/j.epsl.2015.11.041
Simpson, G. D. H. (2006). Modelling interactions between fold-thrust belt deformation, foreland flexure and surface mass transport. *Basin Research*, *18*(2), 125–143. https://doi.org/10.1111/j.1365-2117.2006.00287.x
Stein, R. S., King, G. C. P., & Lin, J. (1994). Stress triggering of the 1994 M=6.7 Northridge, California, earthquake by its predecessors. *Science*, *265*(5177), 1432–1435. https://doi.org/10.1126/science.265.5177.1432
Suppe, J., Chou, G. T., & Hook, S. C. (1992). Rates of folding and faulting determined from growth strata. In K. R. McClay (Eds.), *Thrust tectonics* (pp. 105–121). London: Springer.
Thomson, D. J. (1982). Spectrum estimation and harmonic analysis. *Proceedings of the IEEE*, *70*(9), 1055–1096. https://doi.org/10.1109/PROC.1982.12433
Thomson, D. J. (1990). Time series analysis of Holocene climate data. *Philosophical Transactions of the Royal Society of London, Series A, Mathematical and Physical Sciences*, *330*(1615), 601–616. https://doi.org/10.1098/rsta.1990.0041
Vann, I. R., Graham, R. H., & Hayward, A. B. (1986). The structure of mountain fronts. *Journal of Structural Geology*, *8*(3-4), 215–227. https://doi.org/10.1016/0191-8141(86)90044-1
Vannucchi, P., Remitti, F., & Bettelli, G. (2008). Geologic record of fluid flow and seismogenesis along an erosive subducting plate boundary. *Nature*, *451*(7179), 699–703. https://doi.org/10.1038/nature06486
Wallace, R. E. (1987). Grouping and migration of surface faulting and variations in slip rates on faults in the Great Basin province. *Bulletin of the Seismological Society of America*, *77*, 868–876.
Walsh, J. J., & Watterson, J. (1989). Displacement gradients on fault surfaces. *Journal of Structural Geology*, *11*(3), 307–316. https://doi.org/10.1016/0191-8141(89)90070-9
Wilson, L. F., Pazzaglia, F. J., & Anastasio, D. A. (2009). A fluvial record of active fault-propagation folding, Salsomaggiore anticline, Northern Apennines, Italy. *Journal of Geophysical Research*, *114*, B08403. https://doi.org/10.1029/2008JB005984
Zijderveld, J. D. A. (1967). A.C. Demagnetization of rocks: Analysis of results. In D. W. Collinson, K. M. Creer, & S. K. Runcorn (Eds.), *Methods in paleomagnetism* (pp. 254–286). Amsterdam: Elsevier.